Structural Distortions in Few-Layer Graphene Creases

Alex W. Robertson,[†] Alicja Bachmatiuk,[‡] Yimin A. Wu,[†] Franziska Schäffel,[†] Bernd Büchner,[‡] Mark H. Rümmeli,[‡,§] and Jamie H. Warner[†,*]

[†]Department of Materials, University of Oxford, Parks Road, Oxford OX1 3PH, United Kingdom, [‡]IFW Dresden, P.O. Box 270116, D-01171 Dresden, Germany, and [§]Technische Universität Dresden, D-01062 Dresden, Germany

ABSTRACT

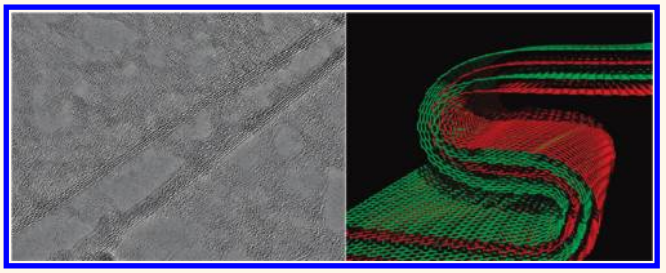

Folds and creases are frequently found in graphene grown by chemical vapor deposition (CVD), due to the differing thermal expansion coefficients of graphene from the growth catalyst and the flexibility of the sheet during transfer from the catalyst. The structure of a few-layer graphene (FLG) crease is examined by aberration-corrected high-resolution transmission electron microscopy (AC-HRTEM). A study of 2D fast Fourier transforms (FFTs) taken about the region of the crease allowed for the crystal stacking structure of the system to be elucidated. It was found that strain-induced stacking faults were created in the AB Bernal-stacked FLG bulk around the region proximal to the crease termination; this is of interest as the stacking order of FLG is known to have an effect on its electronic properties and thus should be considered when transferring CVD-grown FLG to alternate substrates for electronic device fabrication. The FFTs, along with analysis of the real space images, were used to determine the configuration of the layers in the crease itself and were corroborated by multislice atomistic TEM simulations. The termination of the crease part way through the FLG sheet is also examined and is found to show strong out of plane distortions in the area about it.

KEYWORDS: graphene · chemical vapor deposition · APCVD · TEM · HRTEM

The successful growth of graphene, a novel two-dimensional allotrope of carbon with unique electronic properties,[1−3] by chemical vapor deposition (CVD)[4,5] promises for the potential to feasibly incorporate graphene into future applications, such as transparent conducting films in displays. An unavoidable consequence of CVD growth is the attachment of the graphene to the surface of the metal catalyst, such as nickel or copper, which must then be removed in order for the graphene to be isolated and transferred to a desired substrate. A transfer method that is widely used is to apply poly(methyl methacrylate) (PMMA) as a supporting scaffold for the graphene to adhere to, while the underlying metal catalyst is etched.[4,6−8] The PMMA−graphene film can then be transferred to an appropriate substrate, where the PMMA is removed. The nature of the transfer procedure tends to lead to the graphene film being partly cracked[7] and folded,[10−13] arising from the flexible nature of the PMMA−graphene thin film at transfer or from the relaxation and adhesion of the graphene to the new substrate being imperfect. The energetics of the graphene fold system have been found to be dependent on a combination of the van der Waals forces between the overlapping sheets and the stress in the sheets from the bend, with folds along armchair or zigzag directions being energetically preferable.[11] Understanding the atomic structure of defects that form at creases and pleats in graphene layers that develop from the transfer process could be important for future electronic and mechanical applications, where the effects of such defects could be deleterious to their performance.[14,15] We show that a crease termination in a few-layer graphene (FLG) system acts to induce rotational faults between the layers, or turbostratic stacking, in the region nearby. The stacking configuration is known to significantly affect the electronic properties of FLG,[16,17] such as theoretical calculations demonstrating dependence of the Fermi velocity on the rotational angle between layers,[18] and the opening of a band gap due to electronic interactions in ABC configured trilayer graphene systems.[19]

RESULTS AND DISCUSSION

Creasing in the graphene system is evident even before transfer. Figure 1a shows a SEM image of as-grown few-layer graphene on copper foil, with the micrometer-sized

* Address correspondence to jamie.warner@materials.ox.ac.uk.

Received for review October 2, 2011 and accepted November 18, 2011.

Published online November 28, 2011
10.1021/nn203763r

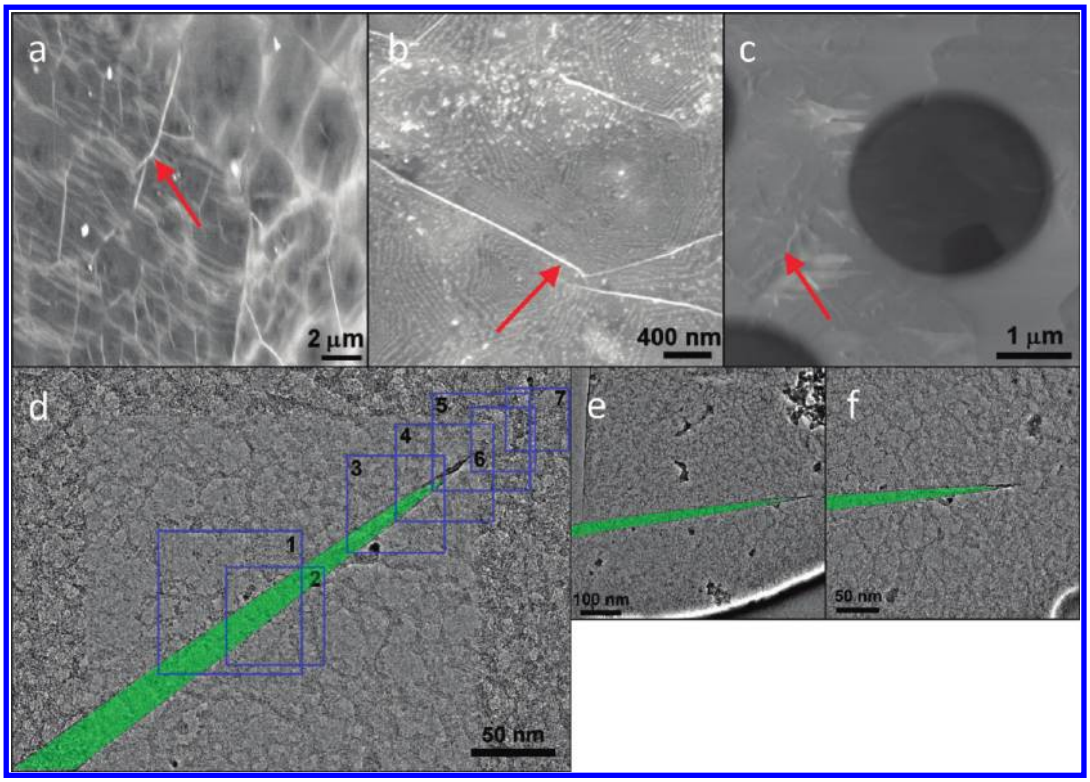

Figure 1. SEM images of (a) FLG as grown on copper, (b) FLG transferred to silicon dioxide, (c) FLG transferred to a holey silicon nitride TEM grid (tilted at 54°). White crease marks (red arrows) are clearly visible in both (a) and (b), and the creasing in (c) is most marked on the left of the hole. (d) TEM image of a crease leading to a single pinch at the top right. The crease is highlighted in green. The numbered blue boxes denote appropriately designated high-magnification regions that are further analyzed later. (e,f) Low-magnification images of the region of the crease, again highlighted in green.

white creases clearly visible. The folds likely occur during the cooling from 1000 °C, with the differing thermal expansion coefficients of graphene to copper leading to the formation of the creases. The transfer process is expected to lead to further creasing due to the flexible nature of the graphene, even when backed with a polymer scaffold. Figure 1b demonstrates this to be so, with a FLG film transferred to a Si:SiO_2 substrate showing multiple creases. From the SEM images, it is evident that the creases all have terminations; it is almost impossible for the typically micrometer-sized creases to form complete folds along the centimeter scale of the complete graphene film. An exception to this is the case where a crease forms with one end terminating at the film edge. A number of creases appear to terminate in the same region, as can be seen in the areas about the red arrows in Figure 1a,b. To study the folds and terminations in more detail, FLG was grown by atmospheric CVD on copper and transferred by the use of a supporting PMMA layer to a holey silicon nitride TEM grid (2 μm diameter holes) (SEM image shown in Figure 1c).[9,20] Further method details are presented in the methodology section. Figure 1d shows a HRTEM image of a crease running across a region of FLG, low-magnification images of which are in Figure 1e,f. The crease diverges from a pinch approximately 500 nm into the film and extends away to the edge, seen on the left of Figure 1e.

To better understand this nontrivial system, it is useful to first investigate some models that could conceivably describe a FLG crease by modeling and TEM simulation. In Figure 2a–i, atomistic models are demonstrated for three different conceivable types of four-layer graphene crease. The first set (Figure 2a–c) shows a simple upward buckle, the second (Figure 2d–f) an overlapping back fold, and the final (Figure 2g–i) a skewed back fold, with a rotation between the layers of the fold. Figure 2j,k,o shows multislice TEM image simulations performed at 7 nm defocus on supercells large enough to fully include the model. The buckle model does not yield the two sets of four interference lines along the fold edges that are observed in the other two simulations; these interference fringes require a complete fold, whereas the buckle model produces a pair of single blurred bands along the steepest regions of the deformation. The inset to Figure 2j shows a 2D fast Fourier transform (FFT) taken from the central area of the crease, showing a single set of six spots at 0.21 nm spacing in a hexagonal configuration, resulting from the six-fold symmetry of the graphene lattice. The angle of the spots in the FFT can be used to determine the armchair direction of the graphene.[13] The back fold model shown in Figure 2d–f yields a pair of interference fringe sets in the simulation, with the FFTs shown displaying a single set of spots with no rotational variation across the crease

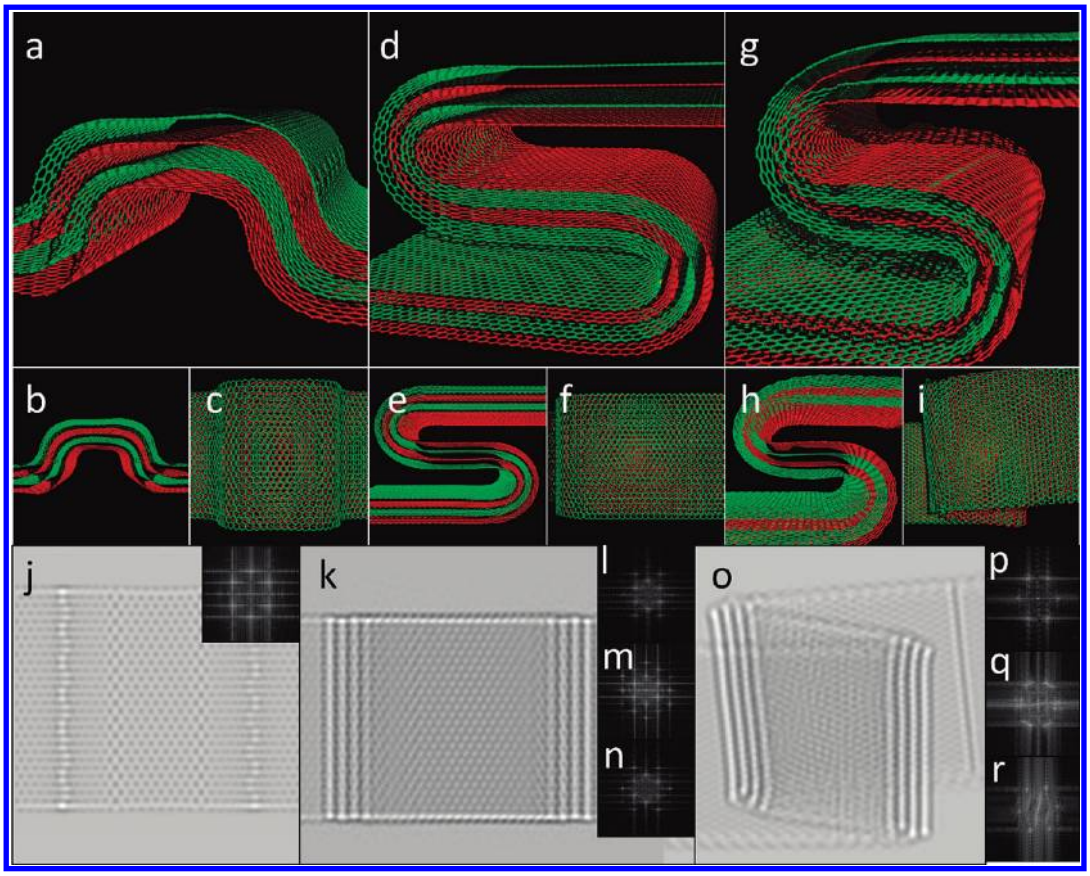

Figure 2. (a−i) Atomistic models of three types of crease, with (a−c) showing an upward buckle in the FLG, (d−f) showing an overlapping back fold, and (g−i) showing a skewed overlapping back fold; a skew of −10° for the bottom layer and 15° for the top with respect to the zigzag direction orthogonal to the middle sheets edge. (j,k,o) Multislice TEM simulations of the buckle (j), overlap (k), and skewed overlap (o) taken at 7 nm defocus. The inset of (j) shows an FFT taken from the central region of the simulation. (l−n) FFTs taken from the left, center, and right parts, respectively, of the simulations in (k). (p−r) FFTs similarly for (o).

region. The model illustrated in Figure 2g−i is skewed such that the bottom layers are rotated by −10° with respect to the middle sheets and the top layers by 15°. The FFTs to the left and right of the fold (Figure 2p,r) show a 25 and 20° rotation from the vertical, with the central region exhibiting a group of blurred spots from approximately 19 to 27°, which likely arises due to the superposition of the two sheets plus a further angle for the intermediate sheet. Unfortunately, the simulation resolution is insufficient to adequately delineate this.

Figure 3a,b shows representative HRTEM images taken from the crease, here corresponding to regions 1 and 5, as defined in Figure 1d. Figure 3c shows a polar map (see inset) of the angle of rotation of the hexagonal spot patterns obtained by FFTs at various locations about the crease, with the rotation vector normalized such that a 60° rotation of spots from the FFT vertical axis corresponds to a 360° rotation in the graphic. FFTs taken from the numbered boxed regions in Figure 3a,b are shown in Figure 3d−k, with Figure 3d−g taken from boxes 1−4 in Figure 3a and Figure 3 boxes 1−4 from Figure 3b. Figure 3d,f,g shows the characteristic set of six spots at 0.21 nm spacing expected for AB Bernal-stacked graphene; however, there is a notable splitting of the spots evident in the FFT shown in Figure 3e, which can be seen from Figure 3a to originate from a region nearer to the central pinch of the fold. The majority of FFTs from Figure 3b, nearer still to the central pinch, demonstrate similar splitting in showing two sets of six spots. This second set of spots originates from the presence of a rotational stacking fault between the graphene layers, with the angle between the spots corresponding to the angle of rotation between the sheets.[21] The stretching of some spots into lines, particularly noticeable in Figure 3h, coincides with a distortion of the graphene sheet such that it is no longer normal to the direction of the electron beam. This arises due to apparently "smaller" lattice spacing in this region, akin to the curved edges of carbon nanotubes.[22] Further discussion of this is presented later. Figure 3a shows two sets of four interference fringes (high-magnification for the top set shown in Figure 3l and the bottom set in Figure 3m) tapering to a single set of four fringes in Figure 3b before terminating (high-magnification in Figure 3n). This result demonstrates that the FLG is four layers thick at the crease.[12]

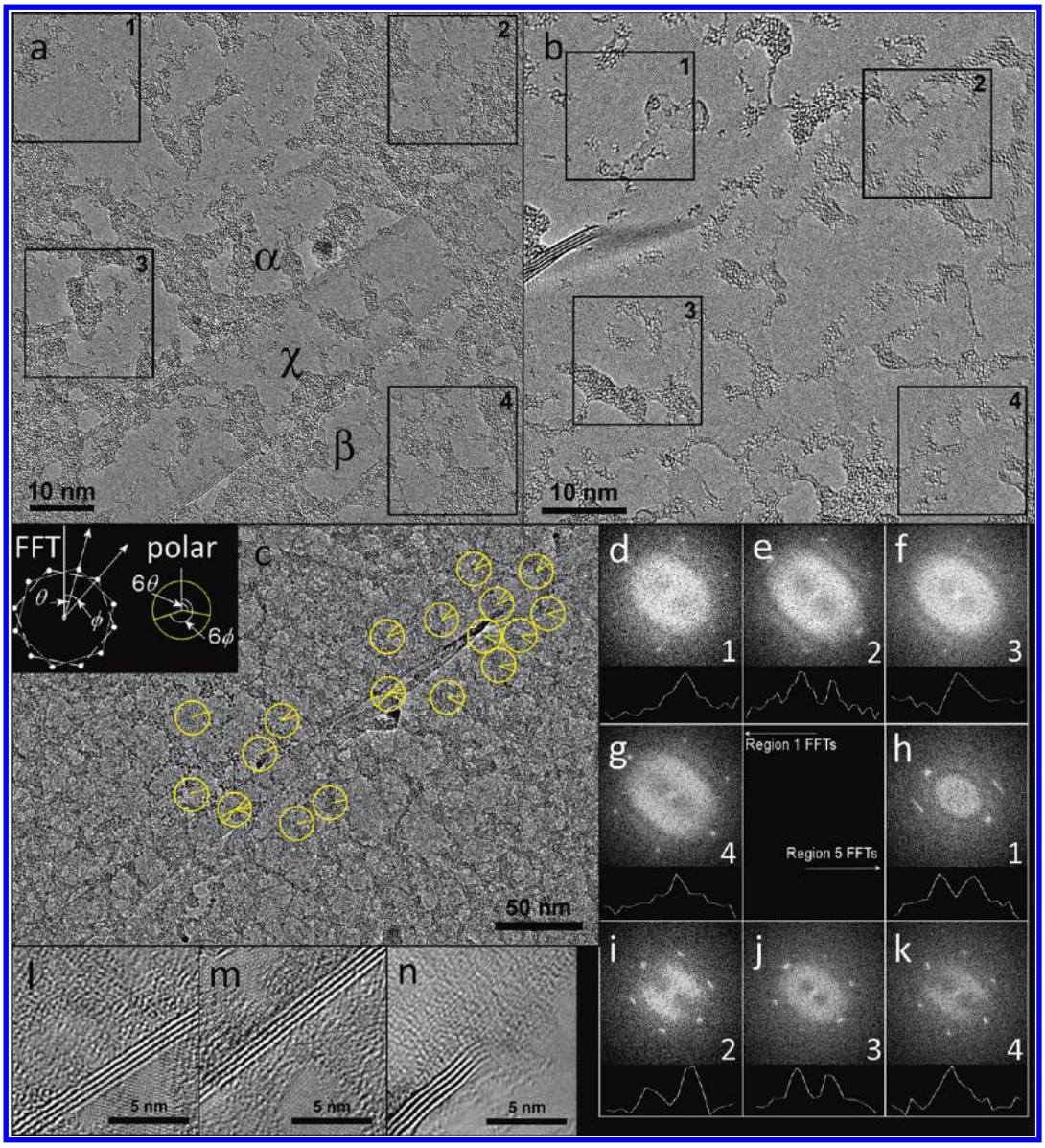

Figure 3. (a,b) HRTEM image of regions 1 and 5, respectively, as defined in Figure 1d. Boxed regions denote areas from which a FFT was taken. The greek letter labels in (a) are used to refer to a particular side of the fold structure. (c) Polar representation (see inset) map of the relative angular rotation of the FFT patterns from the vertical, with the angle normalized to 360°. (d−g) FFTs taken from the corresponding numbered boxes in (a); (h−k) FFTs taken from the numbered boxes in (b). Insets for d−k show intensity line profiles taken across the FFT spots. (l−n) Magnified images from region 1 (l,m) and 5 (n) showing the interference fringes arising from the folding of the graphene.

The map of the relative angles of rotation of the FFT spots shown in Figure 3c demonstrates a splitting of the spots from FFTs taken from either side of the crease within approximately 200 nm of the pinch node. There was no further correlation found between distance from the pinch node and the scale of the rotational misalignment. To further characterize the fold, it becomes necessary to introduce a notation denoting the different areas of the crease. In Figure 3a, the labels α, β, and χ are shown in the top left, bottom right, and central region of the crease, respectively, and shall be referred to when describing FFT angles on different sides of the crease folds. The mean rotation of the spots clockwise from the vertical was found to be $\alpha_a = 11.5 \pm 0.2°$ and $\beta_a = 13.3 \pm 0.3°$ for the top left and bottom right side of the crease, respectively, further from the crease end and before the splitting, with the splitting leading to an extra set of spots appearing at $\alpha_b = 6.0 \pm 0.3°$ for the left and $\beta_b = 19.1 \pm 0.2°$ for the right side. These values are summarized in Table 1. The appearance of the second spot set proximal to the pinch node suggests that the strain in the FLG film about this area is sufficient to induce a shifting in between the layers, resulting in a rotational fault. Some theoretical work has suggested that the translational energy between mutually rotated layers leads to a reduction in the sliding energy between the two layers.[23] As such, it could be that the overall energetics

TABLE 1. Mean of Measured FFT Rotations on the Left (α), Right (β), and Central (χ) Part of the Crease (α_a and β_a Denote the FFT Spots That Are Present before Splitting)

angle from (deg)	α_a	α_b	β_a	β_b	χ_a	χ_b	χ_c	χ_d	χ_e	χ_f
vertical	11.5 ± 0.2	6.0 ± 0.3	13.3 ± 0.3	19.1 ± 0.2	6.9 ± 0.5	11.3 ± 0.3	14.4 ± 0.3	18.8 ± 0.5	36.6 ± 0.2	41.2 ± 0.5
α_a	0	−5.5 ± 0.4	1.8 ± 0.4	7.6 ± 0.3	−4.6 ± 0.5	−0.2 ± 0.4	2.9 ± 0.4	7.3 ± 0.5	25.1 ± 0.3	29.7 ± 0.5

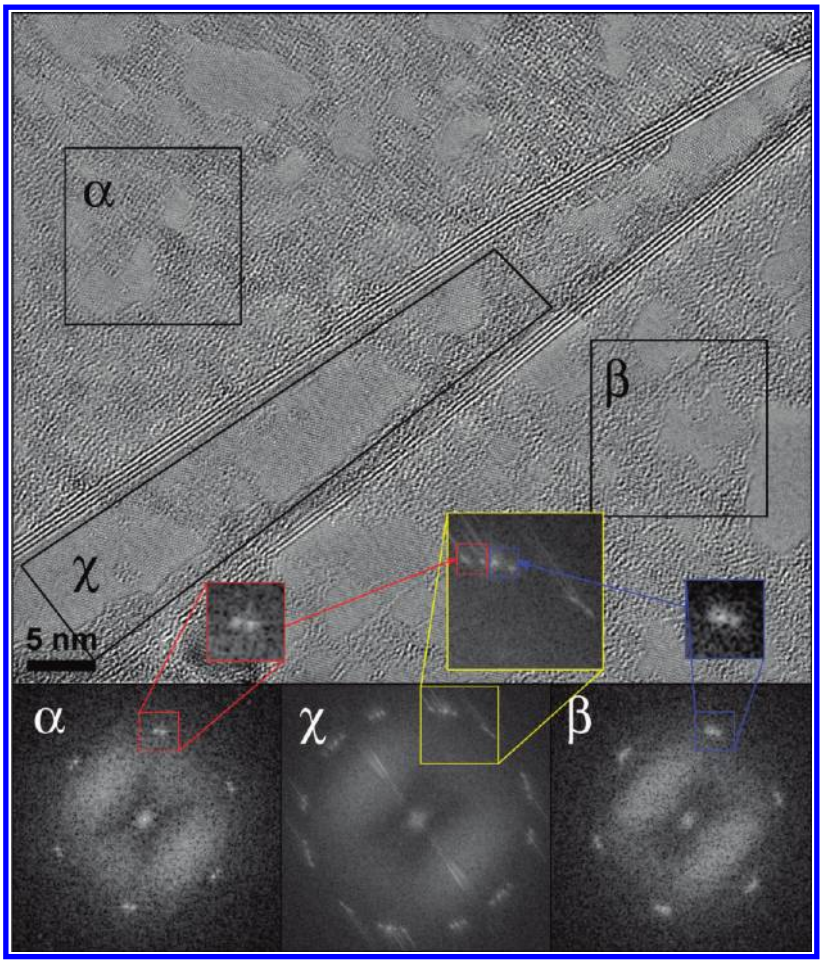

Figure 4. HRTEM image taken from region 3 (Figure 1d). The highlighted areas have corresponding FFT patterns shown underneath, showing two sets, six sets, and two sets of hexagonal spots for α, χ, and β, respectively. Four of the spot sets in χ correspond to the same rotation as the sets seen in α and β.

of the system are made more favorable by the incorporation of this rotational stacking fault, as it would allow for the layers to more freely move across one another to relieve the strain caused by the pinch. FFTs taken further from the pinch node show no such splitting, with the action of the bulk graphene negating the localized strain of the pinch, thus inhibiting the formation of a stacking fault.

Figure 4 shows an image taken from region 3, with FFT patterns extracted from the boxed areas. The patterns in α and β both show rotations in agreement with the averages stated in Table 1; however, the area between the two interference fringes, χ, is of interest in characterizing the nature of the fold type. The FFT shows six sets of hexagonal spots, suggesting that there are six rotational configurations in the actual crease region, more than the two in the regions on either side. However, these are not all stacking faults in a single set of FLG; rather, it is more likely that they are three FLG sheets which each have a single rotational stacking fault, in a configuration similar to the skewed back fold model shown in Figure 2g. This is supported both by four of the FFT spots corresponding with good agreement to rotations found in the regions on either side of the fold region (see Table 1) and by the remaining two spot sets having an average rotation of $\chi_e = 36.6 \pm 0.2°$ and $\chi_f = 41.2 \pm 0.5°$ from the vertical, which when subtracted

by the rotations of the misaligned sheets to the top left of the fold (α_a and α_b) yields values of 30.6 $\pm$ 0.4 and 29.7 $\pm$ 0.5°. This would be in good agreement with the fold being along a zigzag axis in the sheets. Research demonstrating that folds along the armchair and zigzag directions are energetically more favorable support this.[11]

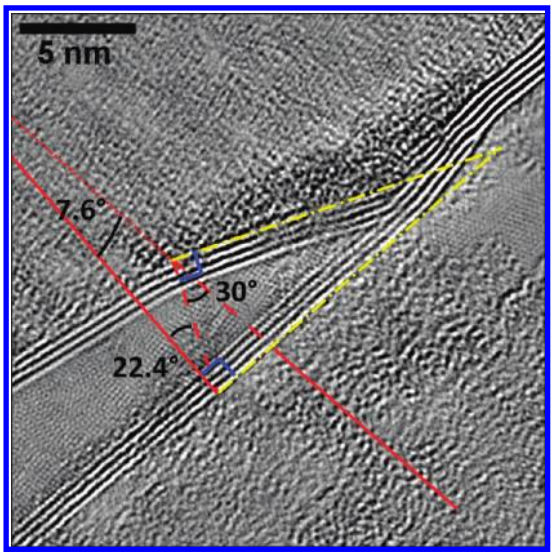

Figure 5. HRTEM image from region 4 including annotations showing the observed rotations in the FLG system across the skewed back fold, with both a 30 and a 22.4° fold, leading to an overall skew of 7.6° across the crease. The yellow dashed lines are orthogonal to the appropriate red lines describing the FLG orientation and can be seen to correlate with the interference fringes originating from the folds in the HRTEM image.

As mentioned, the observed results support the skewed back fold model shown in Figure 2g. This accounts for the fold-induced interference fringes along either side of the crease, the change in relative rotation of the sheets before and after the fold, and the multiple sets of FFT spots observed in the central area of the crease. Finally, the unique FFT spots in the crease region have a relative rotation of 30° to the spots corresponding to the graphene outside the crease, strongly supporting a zigzag fold. On either side of the crease, the angle of the induced rotational stacking fault was found to be 5.5 $\pm$ 0.4° for the α side and 5.8 $\pm$ 0.4° for the β side, suggesting that the same rotational stacking fault propagates through the fold rather than the fold causing discrete defects on either side, which is further supported by the observation of FFT spots with corresponding rotations in χ, as demonstrated in Figure 4. The overall skew of the fold, calculated from the mean difference between the FFT angles for regions α and β, was 7.6 $\pm$ 0.3°. These angles are superimposed on a HRTEM image of the converging crease in Figure 5, showing the correspondence between angles calculated by FFT and the strong distortion leading to the crease node. The red lines represent the relative orientation of the FLG across the crease, with the additional yellow lines taken normal to them at the folds. These can be seen to closely match the imaged folds as it converges toward the end of the

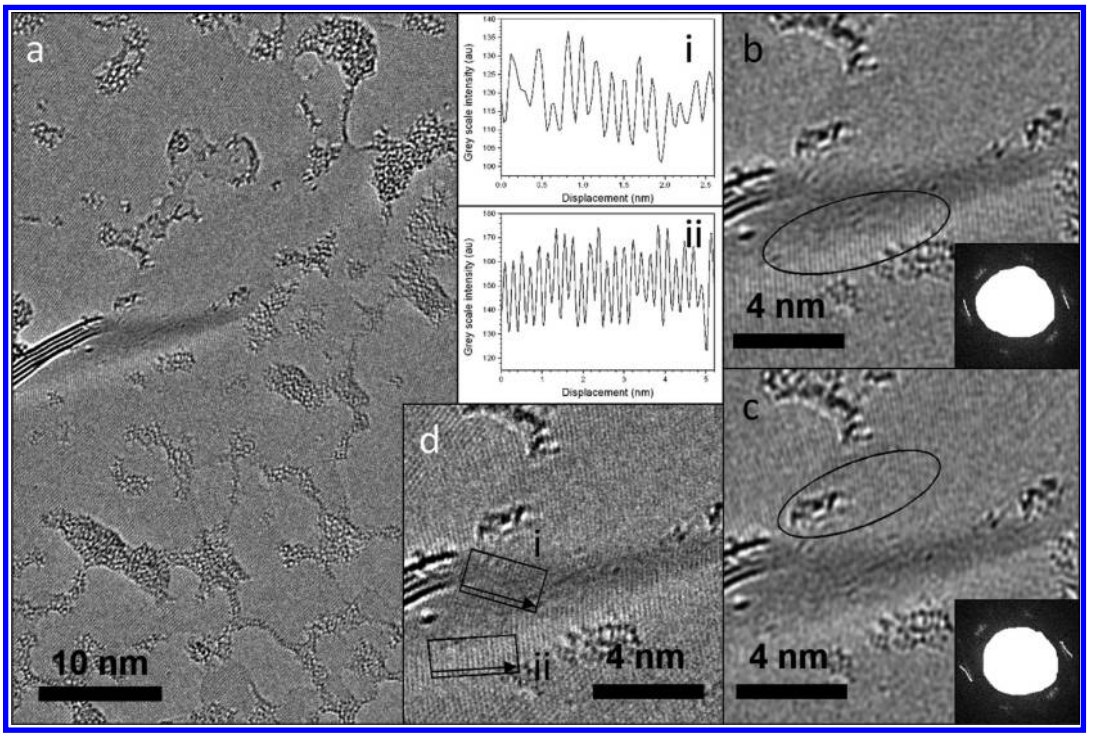

Figure 6. (a) HRTEM image taken from region 5. (b,c) Reconstructed FFT images (FFT positive masks shown in the insets) of (a), showing bending in the graphene lattice lines over and around the shaded region near the fold fringes (circled). (d) Magnified image of the region at the termination of the interference fringes. Box averaged intensity plots are shown, taken from regions labeled i and ii. The arrows correspond to the positive *x*-axis direction.

crease, with a measured angle of 23.1° extracted from the HRTEM image comparing reasonably well to the expected angle of 22.4°.

The low-magnification TEM image of the fold in Figure 1d shows the fold end part way through the graphene film. A HRTEM image of the termination of the fold is displayed in Figure 6a, showing a pronounced band of shadowing to the bottom right of the interference fringes. Reconstruction of positive masked FFTs taken from the area (Figure 6b,c), which selects a specific lattice orientation to display, shows the lines of the graphene lattice bending across the shadowed area. The box averaged intensity profiles are taken from the corresponding labeled boxes in the high-magnification inset to Figure 6a, from the shadow (i) and the light fringe (ii), with the arrow indicating the *x*-axis direction. The boxes were selected to be orthogonal to the direction of the lattice lines, such that measurements of the full width at half-maxima of the peaks from the profiles would yield characteristic lattice distances for the regions. The light fringe lattice spacing was found to be 0.12 and 0.08 nm for the dark fringe. This result is further supported by the streaking evident in the FFT shown in Figure 3h. It is postulated that the change in contrast is similar to a thickness effect, with the out of plane distortion of the graphene being severe enough to lead to a pronounced apparent reduction in the graphene lattice parameter and hence the darker contrast.[24] The strong warping of the graphene in this region would be due to the presence of the fold termination, much as a similar fold in a simple sheet of paper would yield.[25]

CONCLUSION

The structure of a FLG crease has been characterized by HRTEM imaging and simulation. The crease has been shown to be back folded on itself, converging from a shallow skew to one with a 30° fold direction and with a combined skew across the fold of 7.6°. In the high strain region around the end pinch of the FLG crease, severe out of plane distortions were observed, corroborated by direct lattice imaging and measurements, FFT spot stretching, and the observation of pseudothickness originating contrast. What is probably the most important observation for consideration with regards to graphene in applications, however, is the strain-induced stacking faults that have been demonstrated to occur near to the fold pinch. Such stacking faults could have a notable effect on the capabilities of FLG-based devices and illustrate the importance of the fold-inducing transfer step when incorporating CVD graphene grown on copper into a device. Understanding the behavior of folds in graphene is of importance as part of the wider area of study of graphene defects, where their macroscopic effect in electrical devices, and also mechanical systems, will be of interest.

METHOD DETAILS

FLG was synthesized according to a previously reported method.[9] Copper foils (Alfa Aesar, product no. 42189, 99.999% purity) were loaded into a quartz tube located in a horizontal split-tube furnace. After purging the system with argon gas, 600 sccm of a hydrogen/argon gas mix (25% hydrogen) was introduced into the system. At a temperature of 1000 °C, the quartz tube was shifted inward into the furnace, so that the sample resided in the hot zone, where it was annealed and reduced for 30 min to remove surface oxide. A methane/argon gas mixture (20% methane), with a flow rate of approximately 5−10 sccm, was then supplied while continuing to maintain the 600 sccm hydrogen gas mix flow for 3 min. The sample was cooled to ambient temperature by shifting the quartz tube from the furnace and was left to rapidly cool under a hydrogen and argon atmosphere.

For transfer of graphene from the copper foils, an A8 PMMA supportive scaffold (8 wt % in anisole, 495k molecular weight) was spin-coated onto the graphene surface. A spin speed of 4700 rpm was used for 60 s, with the film then cured by heating on a hot plate at 180 °C for 90 s. The underlying copper was etched overnight by an iron(III) chloride solution (concentration of 0.1 g mL^{-1}). The graphene/PMMA film was rinsed in deionized water and transferred to a concentrated hydrochloric acid solution (30%) in order to remove residual contaminants, such as iron from the etching solution. A further thorough rinsing in DI water was then performed. Transfer of the film to a holey silicon nitride TEM grid (Agar Scientific number Y5385) was done by attaching the grid to a lightly sticky pad (Gel-Pak gel-film WF-40-X8-A), which in turn was attached to a glass slide, and using this to "scoop" the film out of the DI water. A further coating of A8 PMMA was applied by drop casting, which acted to relax the graphene film onto the TEM grid, allowing for better adhesion and a better quality transfer of the graphene.[7] This was allowed to dry in air over several hours. The PMMA can be then removed by first applying acetone solvent and then by baking in air for 2−3 h at about 350 °C.

The AC-HRTEM was performed using an aberration-corrected JEOL 2010F microscope operated at 80 kV. Beam current densities were typically in the range of ∼0.0001−0.01 pA nm^{-2}. All shown HRTEM images were subjected to a FFT bandpass filter (ImageJ) to remove low-frequency component associated with non-uniform intensity distribution of the electron beam.

Image simulations were performed using the multislice algorithm in JEMS software using a supercell scaled to include the entire fold model, with a defocus spread of 8 nm, $C_s = -0.005$ mm.

Acknowledgment. J.W. thanks the Royal Society for funding. F.S. thanks the Alexander von Humboldt foundation, the BMBF, and the EPSRC (EP/F048009/1).

REFERENCES AND NOTES

1. Novoselov, K. S.; Geim, A. K.; Morozov, S. V.; Jiang, D.; Katsnelson, M. I.; Grigorieva, I. V.; Dubonos, S. V.; Firsov, A. A. Two-Dimensional Gas of Massless Dirac Fermions in Graphene. *Nature* **2005**, *438*, 197–200.
2. Novoselov, K. S.; Geim, A. K.; Morozov, S. V.; Jiang, D.; Zhang, Y.; Dubonos, S. V.; Grigorieva, I. V.; Firsov, A. A. Electric Field Effect in Atomically Thin Carbon Films. *Science* **2004**, *306*, 666–669.
3. Novoselov, K. S.; Morozov, S. V.; Mohinddin, T. M. G.; Ponomarenko, L. A.; Elias, D. C.; Yang, R.; Barbolina, I. I.; Blake, P.; Booth, T. J.; Jaing, D.; *et al.* Electronic Properties of Graphene. *Phys. Status Solidi B* **2007**, *244*, 4106–4111.

4. Kim, K. S.; Zhao, Y.; Jang, H.; Lee, S. Y.; Kim, J. M.; Kim, K. S.; Ahn, J. H.; Kim, P.; Choi, J. Y.; Hong, B. H. Large-Scale Pattern Growth of Graphene Films for Stretchable Transparent Electrodes. *Nature* **2009**, *457*, 706–710.
5. Li, X.; Cai, W.; An, J.; Kim, S.; Nah, J.; Yang, D.; Piner, R.; Velamakanni, A.; Jung, I.; Tutuc, E.; *et al.* Large-Area Synthesis of High-Quality and Uniform Graphene Films on Copper Foils. *Science* **2009**, *324*, 1312–1314.
6. Reina, A.; Jia, X.; Ho, J.; Nezich, D.; Son, H.; Bulovic, V.; Dresselhaus, M. S.; Kong, J. Large Area, Few-Layer Graphene Films on Arbitrary Substrates by Chemical Vapor Deposition. *Nano Lett.* **2009**, *9*, 30–35.
7. Li, X.; Zhu, Y.; Cai, W.; Borysiak, M.; Han, B.; Chen, D.; Piner, R. D.; Colombo, L.; Ruoff, R. S. Transfer of Large-Area Graphene Films for High-Performance Transparent Conductive Electrodes. *Nano Lett.* **2009**, *9*, 4359–4363.
8. Yu, Q.; Jauregui, L. A.; Wu, W.; Colby, R.; Tian, J.; Su, Z.; Cao, H.; Liu, Z.; Pandey, D.; Wei, D.; *et al.* Control and Characterization of Individual Grains and Grain Boundaries in Graphene Grown by Chemical Vapour Deposition. *Nat. Mater.* **2011**, *10*, 443–449.
9. Robertson, A. W.; Warner, J. H. Hexagonal Single Crystal Domains of Few-Layer Graphene on Copper Foils. *Nano Lett.* **2011**, *11*, 1182–1189.
10. Kim, K.; Lee, Z.; Malone, B. D.; Chan, K. T.; Alemán, B.; Regan, W.; Gannet, W.; Crommie, M. F.; Cohen, M. L.; Zettl, A. Multiply Folded Graphene. *Phys. Rev. B* **2011**, *83*, 245433.
11. Zhang, J.; Xiao, J.; Meng, X.; Monroe, C.; Huang, Y.; Zuo, J. M. Free Folding of Suspended Graphene Sheets by Random Mechanical Stimulation. *Phys. Rev. Lett.* **2010**, *104*, 166805.
12. Meyer, J.; Geim, A.; Katsnelson, M. I.; Novoselov, K. S.; Booth, T. J.; Roth, S. The Structure of Suspended Graphene Sheets. *Nature* **2007**, *446*, 60–63.
13. Warner, J. H.; Rümmeli, M. H.; Gemming, T.; Büchner, B.; Briggs, G. A. D. Direct Imaging of Rotational Stacking Faults in Few Layer Graphene. *Nano Lett.* **2009**, *9*, 102–106.
14. Rainis, D.; Taddei, F.; Polini, M.; León, G.; Guinea, F.; Fal'ko, V. I. Gauge Fields and Interferometry in Folded Graphene. *Phys. Rev. B* **2011**, *83*, 165403.
15. Ambrosi, A.; Bonanni, A.; Pumera, M. Electrochemistry of Folded Graphene Edges. *Nanoscale* **2011**, *3*, 2256–2260.
16. Mak, K. F.; Sfeir, M. Y.; Misewich, J. A.; Heinz, T. F. The Evolution of Electronic Structure in Few-Layer Graphene Revealed by Optical Spectroscopy. *Proc. Natl. Acad. Sci. U.S.A.* **2010**, *107*, 14999–15004.
17. Mak, K. F.; Shan, J.; Heinz, T. F. Electronic Structure of Few-Layer Graphene: Experimental Demonstration of Strong Dependence on Stacking Sequence. *Phys. Rev. Lett.* **2010**, *104*, 176404.
18. Shallcross, S.; Sharma, S.; Kandelaki, E.; Pankatov, O. A. Electronic Structure of Turbostratic Graphene. *Phys. Rev. B* **2010**, *81*, 165105.
19. Bao, W.; Jing, L.; Velasco, J.; Lee, Y.; Liu, G.; Tran, D.; Standley, B.; Aykol, M.; Cronin, S. B.; Smirnov, D.*et al.*. Stacking-Dependent Band Gap and Quantum Transport in Trilayer Graphene. *Nat. Phys.* **2011**, DOI: 10.1038/nphys2103.
20. Robertson, A. W.; Bachmatiuk, A.; Wu, Y. A.; Schäffel, F.; Rellinghaus, B.; Büchner, B.; Rümmeli, M. H.; Warner, J. H. Atomic Structure of Interconnected Few-Layer Graphene Domains. *ACS Nano* **2011**, *5*, 6610–6618.
21. Warner, J. H.; Schäffel, F.; Rümmeli, M. H.; Büchner, B. Examining the Edges of Multi-layer Graphene Sheets. *Chem. Mater.* **2009**, *21*, 2418–2421.
22. Lucas, A. A.; Bruyninckx, V.; Lambin, P.; Bernaerts, D.; Amelinckx, S.; Landuyt, J. V.; Tendeloo, G. V. Electron Diffraction by Carbon Nanotubes. *Scanning Microsc.* **1998**, *12*, 415–436.
23. Shallcross, S.; Sharma, S.; Pankatrov, O. A. Twist Boundary in Graphene: Energetics and Electric Field Effect. *J. Phys.: Condens. Matter.* **2008**, *20*, 454224.
24. Horiuchi, S.; Gotou, T.; Fujiwara, M.; Ryuji, S.; Hirata, M.; Kimoto, K.; Asaka, T.; Yokosawa, T.; Matsui, Y.; Watanabe, K. Carbon Nanofilm with a New Structure and Property. *Jpn. J. Appl. Phys.* **2003**, *42*, L1073–L1076.
25. Vandeparre, H.; Piñeirua, M.; Brau, F.; Roman, B.; Bico, J.; Gay, C.; Bao, W.; Lau, C. N.; Reis, P. M.; Damman, P. Wrinkling Hierarchy in Constrained Thin Sheets from Suspended Graphene to Curtains. *Phys. Rev. Lett.* **2011**, *106*, 224301.